LA-UR- 93-1670

Title: MICROMECHANICAL STRENGTH EFFECTS IN SHOCK COMPRESSION OF SOLIDS

Author(s): J. N. Johnson

Submitted to: APS/AIRAPT
June 28 - July 3, 1993
Colorado Springs, CO

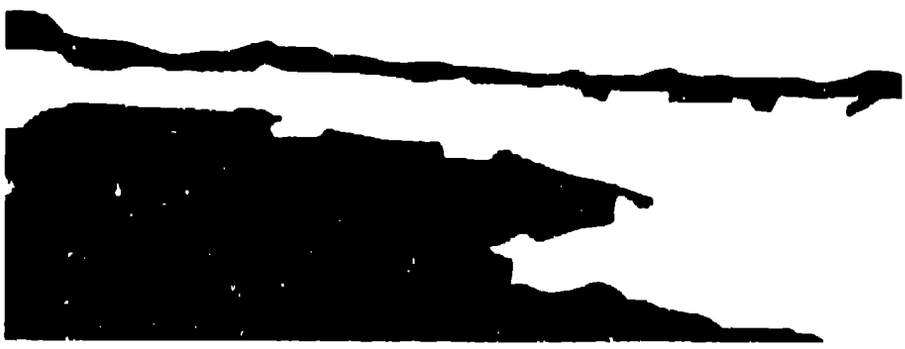

Los Alamos
NATIONAL LABORATORY

MICROMECHANICAL STRENGTH EFFECTS IN SHOCK COMPRESSION OF SOLIDS

J. N. Johnson
Los Alamos National Laboratory
Los Alamos, New Mexico, USA 87545

Time-resolved shock-wave measurements and post-shock recovery techniques have long been used as means of inferring the underlying micromechanics controlling high-rate deformation of solids. This approach requires a considerable amount of subjective interpretation. In spite of this feature, progress has been made in experimentation and theoretical interpretation of the shock-compression/release cycle and some of the results are reviewed here for weak shocks. Weak shocks are defined to be those with peak amplitudes (typically 10 - 20 GPa for most solids) that do not overdrive the elastic precursor. The essential elements of a typical shock-compression/release cycle involve, in order, (a) the elastic precursor, (b) plastic loading wave, (c) pulse duration, (d) release wave, and (e) post-mortem examination. These topics are examined in turn, with some emphasis given to elements (b) and (d). If the plastic loading wave is traveling without change of shape, it is possible to convert the particle-velocity/time records to a shear-stress/plastic-strain-rate path. Shock data in this form can be compared directly with low-t -intermediate strain-rate tests. Results for copper and tantalum show how shock data can be used to determine the transition from the deformation mechanism of thermal activation to that of dislocation drag. An important result of release-wave studies is that the leading observable release disturbance in FCC metals may not be propagating with the ideal, longitudinal elastic-wave speed, but at a lower velocity dependent on the elastic bulk and shear moduli and the product of the dislocation density times the pinning separation squared for dislocation segments in the region behind the shock and ahead of the release wave.

INTRODUCTION

How can an experimentalist look inside a shock-loaded solid on a submicrosecond time scale and examine the micromechanical aspects of material strength and deformation properties? The answer seems to be that general direct observation is very difficult except for a few special materials, and then only for a few special phenomena that can be probed by clever optical means [1-3]. This means that most of our "information" concerning the micromechanical basis for material deformation under shock conditions must come from indirect methods. Measurement of particle velocity, longitudinal stress, impulse, and so on, contains information about the microstructure, if the data can be interpreted properly.

The interpretation of macroscale measurement to provide microscale information is a difficult and nonunique process. This was recognized by Orowan, one of the co-discoverers of the dislocation [4]; and he expressed his reservations about being able to discern the micromechanical basis of material deformation from integral tensile tests as follows:

> *". The extension of a piece of metal (is) in a sense more complicated than the working of a pocket watch and to hope to derive information about its mechanism from . the tensile test (is) perhaps as optimistic as would be an attempt to learn about the working of a pocket watch by determining its compressive strength "*

In spite of this very discouraging viewpoint, I want to describe some positive things that have been done to shed light on the micromechanical basis for material deformation and plastic flow in shock loaded solids. There has been some progress, but it has taken a long time and a great deal of resources, and current interpretations remain open to further investigation.

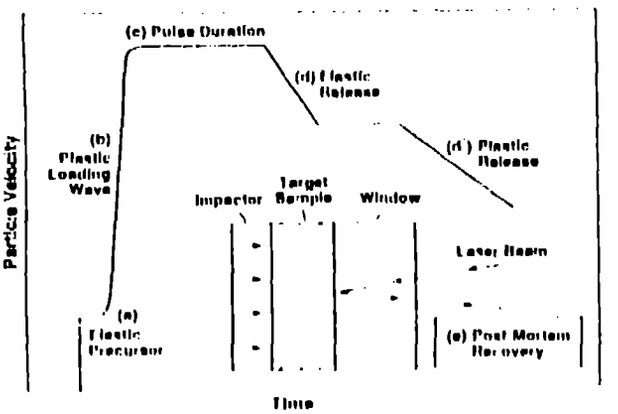

Figure 1. Plate impact experiment

Figure 1 shows an idealized flat plate impact profile of particle velocity as a function of time at some hypothetical gage location interior to the sample. If the sample material is transparent, these measurements can be made *in situ*. More often, as in the case of metals, measurements are made at the planar interface between the sample and a transparent window material chosen to provide a reasonably good acoustic impedance match with the sample. When an approximate impedance match is obtained, spallation is prohibited, the idealized record shown in Figure 1 contains no information about tensile fracture properties of solids, that is a topic for separate discussion.

The main features of the wave profile shown in Figure 1 are (a) the elastic precursor, (b) the plastic compression wave, (c) the nominally flat plateau between compression and release, (d) the elastic-plastic release wave, and (e) post-mortem recovery (following the shock/release cycle). I will deal with each of these topics in turn, with emphasis on (b) and (d).

The micromechanical basis for high-rate plastic deformation is extremely complex. In order to make sense of indirect experimental observations, we need a simplified picture of the deformation process. Figure 2 shows some of the major aspects of plastic deformation on the mesoscale. Pictured here are several dislocation line segments traversing a principal glide plane. The intersections of the straight lines in the glide plane represent atomic positions in a simple cubic lattice. Of course when we consider glide on (111) planes in <110> directions of the FCC lattice, atomic positions are more complicated than this. Also shown in the glide plane are pinning obstacles provided by impurities, interstitials, and other dislocations.

Three major factors contribute resistance to dislocation motion; **(a) the pinning obstacles, (b) the static resistance of the lattice itself (Peierls stress),** and **(c) the drag resistance** provided by the lattice when the applied stress exceeds the Peierls stress and the dislocation is running in the clear region between pinning obstacles. In this picture (a) and (b) are thermally activated processes, and (c) is a simple mechanical dissipative process.

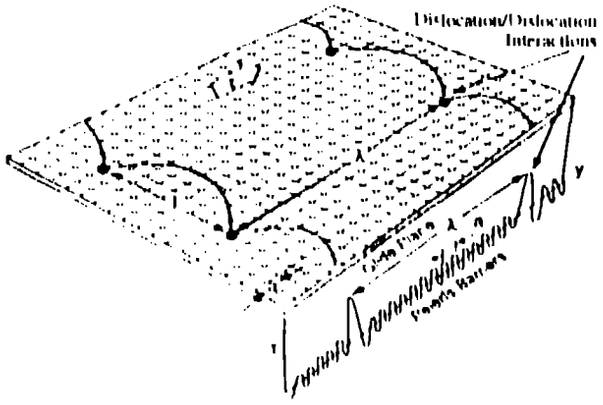

Figure 2. Schematic representation of plastic deformation mechanisms.

Omitted from this diagram are important effects such as dislocation climb, in which a pinned dislocation can climb out of the principal glide plane by cross slip on an intersecting plane, for example. Nevertheless, the simplified picture shown in Figure 2 provides a means of interpreting shock wave response as shown in Figure 1. What I intend to present is a broad interpretation of how and when **deformation mechanisms (a), (b), and (c)** contribute to mechanical strength effects in shock wave compression of FCC and BCC metals, and how the bowed out dislocation segments between pinning obstacles contribute to quasielastic behavior in the "elastic" portion of the elastic-plastic release wave.

COMPRESSION/RELEASE PROFILE

Elastic Precursor

This aspect of shock compression has received a great deal of study, particularly experimental measurement of LiF single crystals [5-7]. Deformation at the elastic precursor front is controlled by **mechanism (c)**, with a great deal of mobile dislocation multiplication. The elastic precursor undergoes extreme excursions in applied shear stress near the impact surface, and for this reason is very hard to characterize fully. Important aspects of the decaying elastic precursor have been reviewed in reference [8].

Plastic Compression Wave

The plastic compression wave is even more complicated in its deformation processes than the elastic precursor, but has seen greater success in micromechanical interpretation.

The important aspect of the plastic compression wave that allows analysis is the fact that it very quickly establishes a steady propagating profile; that is, the particle velocity in the plastic-wave region can be expressed as a function of $x - Ut$, where U is the shock velocity corresponding to that particular wave amplitude. The rule of thumb [9] is that the transit time to steady propagation is ~ 15 risetimes of the plastic wave front. For example, if the risetime of a 7.3 GPa shock in tantalum is 30 ns, the steady nature of the plastic wave is established in less than 500 ns (propagation distance of ~2 mm). Of course it is always better to establish steady-wave behavior experimentally if the resources are available, but this is not always possible.

When the plastic wave is steady, the longitudinal stress, specific volume, and particle velocity satisfy the mass- and momentum-conservation relationships:

$$\varepsilon = 1 - V/V_0 = u/U \quad , \tag{1}$$

$$\sigma = \rho_0 U u \quad . \tag{2}$$

If u and U are known, ε and σ can be obtained. If additional equation of state information is known, it is also possible to obtain the shear stress τ and the longitudinal plastic strain ψ [10-12]. This is the computationally intensive part of the problem. But the important result is that we can then plot the shock data in terms of shear stress, plastic strain, and plastic strain rate. This is the common currency of materials scientists. We do not have to run a hydrocode and show agreement between theory and experiment in order to convince someone that we know the mechanism responsible for shock deformation. The data are simply plotted in the (τ, ψ), $(\psi, \dot{\psi})$, or $(\tau, \dot{\psi})$ planes and the interpretation is almost immediate.

For example, shock compression of copper shows the distinct transition to viscous dislocation drag, mechanism (c), before returning to the thermal activation **mechanism (a)** in the region behind the shock front (Figure 3). The upper solid curves represent the actual τ, ψ paths [13] followed in the shock fronts, while the lower dash and

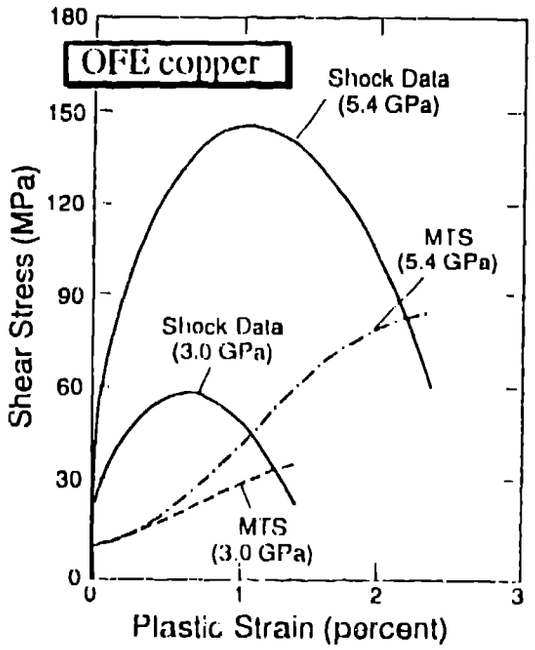

Figure 3. Shear stress paths in shock compression experiments (OFE copper). MTS values are calculated from measured plastic strain rates.

dash dot paths give the mechanical threshold stress (MTS) as a function of ψ through two different shock paths. The MTS is the 0 K shear strength, and the actual thermally activated flow stress is somewhat less than this due to finite temperature [14]. At the end of the shock path the shear stress falls below the MTS and the deformation mechanism reverts to thermal activation.

An important question is: what region of ψ, $\dot{\psi}$ space is dominated by thermal activation as compared to viscous drag in OFE copper? The answer is that at high strain rates and low plastic strains viscous dislocation drag, **mechanism (c)**, controls material deformation. As deformation proceeds, the MTS increases due to rate dependent work hardening, **mechanism (a)**, and eventually overtakes the viscous drag contribution. Hence, for this material, viscous drag plays a dominant role only in the shock front.

Tantalum has also been studied as a typical BCC metal, and it is of interest to determine the dominant deformation mechanisms under various loading conditions. Figure 4 shows shock compression data [15] in comparison with Hopkinson bar measurements over several decades in plastic strain rate. The flat plateau region on the right is the Peierls stress (~0.48 GPa). Without other deformation mechanisms there would be no resistance to applied shear stress above the Peierls stress. The dashed line rising very steeply at a plastic strain rate on the order of 10^5 s^{-1} is based on the theory of linear dislocation drag with constant

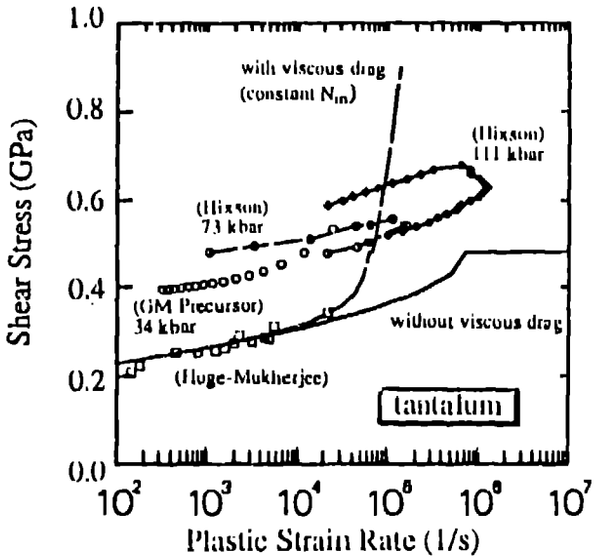

Figure 4. Shear stress paths in shock compression and Hopkinson bar experiments (tantalum).

mobile dislocation density N_m. The experimental shock data clearly show the importance of rapid mobile dislocation density evolution, and a very strong dependence of plastic strain rate on shear stress in the viscous drag regime. We currently have no constitutive models that adequately represent this material behavior.

It is also clear from the data shown in Figure 4 that thermal activation through the Peierls barriers and viscous dislocation drag, **mechanisms (b) and (c)**, have about the same strain rate sensitivity, and that there is no clear distinction between the two deformation mechanisms as there is for OFE copper. At larger plastic strains dislocation/dislocation interactions also play a role in determining material strength of tantalum.

Pulse Duration Effects

The region between compression and release is usually thought of as being nearly constant, without much in the way of microstructural evolution. This appears to be incorrect, based on the numerous observations of pulse duration having an influence on post shock material strength. Reference [8] contains some added discussion on the possible origins for this effect.

Quasielastic Release

Just as analysis of the elastic precursor can yield information on micromechanical behavior in the vicinity of the initial state, unloading (or reloading) waves contain micromechanical information about the shocked state. In fact, some things simplify the analysis of release waves and other things make it more complicated. Since the sound

speed generally increases with compression, the shear stress in the release wave does not undergo the extreme excursion that it does in the precursor. However, the release wave is moving into pre-shocked material for which we have very little direct information about existing microstructure (dislocation density, pinning separation, etc), and speculation and conjecture therefore become a little more important than we would like.

Nevertheless, something can be said about release from the shocked state [16,17]. These effects are simply summarized here.

The source of quasielastic release is the pinned dislocation segments shown in Figure 2. Because of dislocation curvature there is a back stress $\beta = Gb/R$, where R is the radius of curvature of the segment, acting in opposition to the applied shear stress τ. As the shear stress is reduced in the release wave, the pinned dislocation segment immediately sweeps out area in the reverse direction (as it collapses toward straight equilibrium between the two pinning points) and contributes to reverse plastic flow.

This effect can be quantified, and the quasielastic release wave profile calculated as shown for OFE copper in Figure 5 [16] using a linearized version of the evolutionary equations. The nondimensional micromechanical constants for this calculation are $B/(nb^2) = 0.002$ GPa ns and $B(L/b)^2 = 0.005$ GPa ns, where B is the viscous drag coefficient, n is the density of pinned segments, L is their pinning separation and b is the magnitude of the Burgers vector. The results shown in Figure 5 are not the whole story, but it does give an indication of the kinds of things that can be learned about micromechanics from release waves.

An important aspect of release wave behavior in FCC metals is that the leading observable release may not correspond to fully elastic behavior [17]. Instead of sampling the longitudinal modulus $K + 4G/3$ in the shock-compressed state, the leading observable release wave is determined by $K + (4G/3)[1 + nL^2/4]^{-1}$. Since we have little control over the product nL^2 in a shock experiment, care should be exercised in using release wave data to determine elastic moduli in FCC metals.

Post Mortem Recovery

Important information on material microstructure can also be obtained from careful recovery experiments. The drawbacks of these experiments are that some additional deformation occurs in the release wave and perhaps in the catching process itself. However, an actual view of the microstructure, even post mortem, is often very helpful in eliminating false mechanisms from real time data interpretation. The review article by Gray [18] describes the recovery process and the kinds of information that can be obtained.

SUMMARY

In spite of complex material behavior and incomplete experimental data, shock compression scientists have been able to piece together a consistent micromechanical picture of high rate deformation. Direct observation of these processes would greatly aid in establishing uniqueness of interpretation.

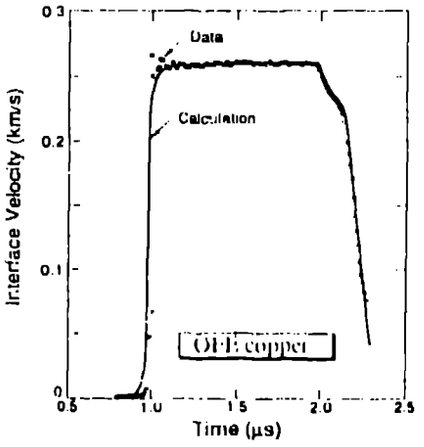

Figure 5. Comparison of experimental data and calculation of quasielastic release in OFE copper shocked to 10 GPa.

REFERENCES

[1] J. S. Wark, R. R. Whitlock, A. A. Hauer, J. E. Swain, and P. J. Solone, *Phys. Rev. B* **40**, pp. 5705-5714 (1989).

[2] P. D. Horn and Y. M. Gupta, *Phys. Rev. B* **39**, pp. 973-979 (1989).

[3] D. S. Moore and S. C. Schmidt, in *Shock Waves in Condensed Matter 1987* (edited by S. C. Schmidt and N. C. Holmes), Amsterdam: Elsevier, 1988, pp. 35-42.

[4] E. Orowan, *Proc. Instn. Mech. Engrs.* **151**, pp. 133-141 (1944).

[5] J. R. Asay, G. R. Fowles, G. E. Duvall, M. H. Miles, and R. F. Tinder, *J. Appl. Phys.* **43**, pp. 2132-2145 (1972).

[6] Y. M. Gupta, G. E. Duvall, and G. R. Fowles, *J. Appl. Phys.* **46**, pp. 532-546 (1975).

[7] G. Meir and R. J. Clifton, *J. Appl. Phys.* **59**, pp. 124-148 (1986).

[8] J. N. Johnson, in *High Pressure Shock Compression of Solids* (edited by J. R. Asay and M. Shahinpoor), New York: Springer-Verlag, 1993, ch. 1.

[9] D. L. Tonks, personal communication (1992).

[10] D. C. Wallace, *Phys. Rev. B* **22**, pp. 1487-1494 (1980).

[11] D. C. Wallace, Los Alamos Rep. LA-10119 (1985).

[12] D. Tonks, Los Alamos Rep. LA-12068-MS (1991).

[13] J. N. Johnson and D. L. Tonks, in *Shock Waves in Condensed Matter 1991* (edited by S. C. Schmidt, R. D. Dick, J. W. Forbes, and D. G. Tasker) Amsterdam: Elsevier, 1992, pp. 371-378.

[14] P. S. Follansbee and U. F. Kocks, *Acta Metall.* **36**, pp. 81-93 (1988).

[15] D. L. Tonks, R. S. Hixson, J. N. Johnson, and G. T. Gray III, this volume.

[16] J. N. Johnson, R. S. Hixson, G. T. Gray III, and C. E. Morris, *J. Appl. Phys.* **72**, pp. 429-441 (1992).

[17] J. N. Johnson, J. Phys. Chem. Solids (in press, 1992).

[18] G. T. Gray III, in *High Pressure Shock Compression of Solids* (edited by J. R. Asay and M. Shahinpoor), New York: Springer-Verlag, 1993, ch. 6.